

Development of an Inspection Process for Ball-Grid-Array Technology Using Scanned-Beam X-Ray Laminography

S. M. Rooks, B. Benhabib, *Member, IEEE*, and K. C. Smith, *Fellow, IEEE*

Abstract—An inspection process based on scanned-beam X-ray laminography (SBXLAM) is proposed herein for quantitatively monitoring the quality of ball-grid-array (BGA) joints. The long-term reliability of the BGA joints depends on the component-assembly process producing joints with sufficient solder volume and proper alignment.

Inspection algorithms were developed to measure the critical BGA-joint characteristics, including the alignment between the ball and the PCB pad, the solder thickness, and the average joint-diameter, and thus, determine whether the joints are defective. The performance of the inspection algorithms was evaluated by inspecting samples with defects that were independently verified.

Index Terms—Solder-joint inspection, X-ray laminography.

I. INTRODUCTION

A. Overview

CONTINUAL increases in IC-chip complexity and performance are placing demands on the density and functionality of package I/Os. Therefore, various SMT interconnection techniques are being developed to satisfy this need, including Ball-Grid-Array (BGA) [1]. BGA is an area-array interconnection that can achieve a density of 400 I/Os per square inch. Referring to Fig. 1, the particular BGA structure investigated consists of high-temperature, lead/tin solder balls that are attached to pads on both the PCB and the bottom side of the ceramic chip package with eutectic tin/lead solder.

The solder-joint volume and ball/pad alignment are the most critical characteristics that the BGA-assembly process must consistently produce to ensure reliability. Furthermore, the BGA-assembly process must be controlled to minimize such process defects as pad nonwets and solder bridges. To develop and control such a robust assembly process requires using an inspection technique to characterize the process.

B. Solder-Joint Inspection Techniques

It is envisioned that the inspection technique, chosen to monitor the quality of BGA joints, must be able to accurately detect the possible BGA-process defects and also have a desired inspection rate of about 15 joints per second.

Manuscript received June 1994; revised June 5, 1995.

The authors are with the Computer Integrated Manufacturing Laboratory, Department of Mechanical Engineering, University of Toronto, ON M5S 1A4, Canada.

IEEE Log Number 9415585.

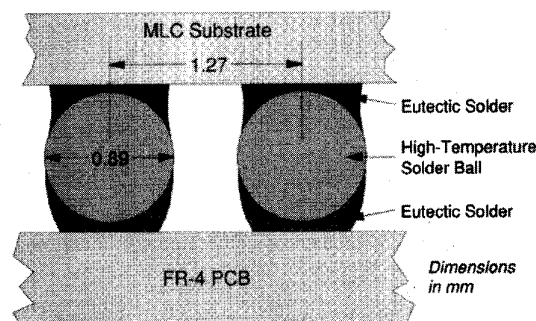


Fig. 1. Basic ball-grid-array structure.

Various automated solder-inspection systems are commercially available for monitoring solder-joint quality. The techniques used in these systems can be characterized by the radiation employed (either infrared, visible light, X-ray, or acoustic), the way in which the radiation interacts with the object being inspected, and the means used to detect the response of the radiation [2]–[6]. Only techniques utilizing penetrating radiation, such as acoustic and X-ray, could possibly inspect all BGA joints within the area array. However, acoustic microscopy is not suitable for consistently inspecting BGA joints due to the possibility of air gaps existing along the path of the propagating ultrasound-wave within the chip package, as well as the highly-attenuating chip substrate itself [3]. Therefore, only X-ray systems were seriously considered for inspecting BGA joints.

Transmission X-ray systems operate on the principle that solder attenuates the intensity of an X-ray photon-beam to a much greater degree than any other material present in a PCB assembly, such as copper, FR-4, or metallized ceramic [4]. However, in being transmissive, the intensity of the X-ray image is due to the *combined* attenuation of the X-ray beam by every feature along its path. With respect to BGA joints, the supporting solder ball with its high-lead content would entirely obscure the eutectic-solder fillets in a transmission X-ray image. Transmission X-ray systems, therefore, cannot be used to inspect the quality of BGA joints.

In order to inspect the eutectic-solder fillets of BGA joints using an X-ray system, the system must be able to focus on a particular horizontal cross-sectional plane and, therefore, isolate the solder fillets from the solder balls. Scanned-beam X-ray laminography (SBXLAM) is the only automated X-ray

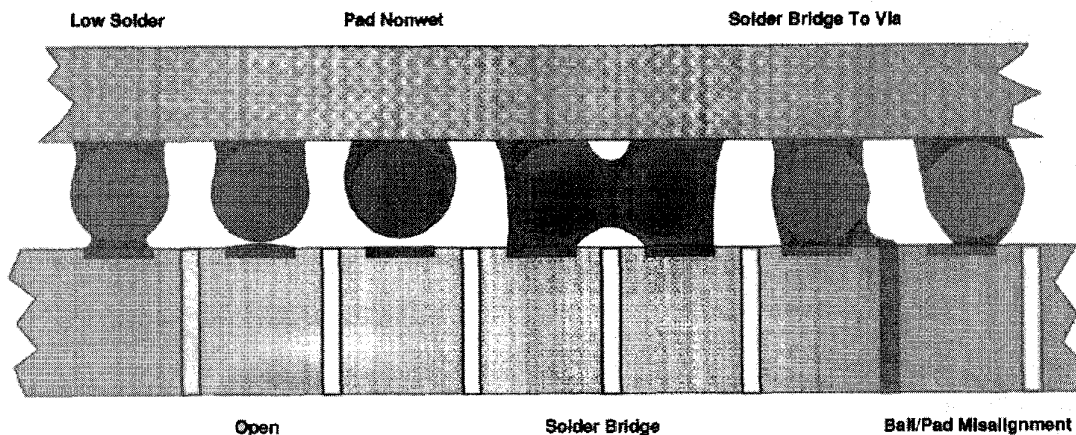


Fig. 2. Defective BGA joints.

technique currently capable of focusing on a horizontal plane to examine features within this plane with great detail and contrast [6], [7]. The success of SBXLAM is based not only on detecting defects but also on measuring solder-joint characteristics to provide process-control data. Amongst electronics companies, Fujitsu has successfully used an SBXLAM system for inspecting solder-bump connections between LSI modules and ceramic PCB's [8]. Both IBM [9] and Hitachi [10] have also had success with using the system to inspect *J*-lead solder joints. Research on TAB-joint inspection using an SBXLAM system was reported in [11]. Based on the above mentioned capabilities, the SBXLAM approach was chosen for the X-ray system utilized to perform the automated inspection of BGA joints.

II. INSPECTION REQUIREMENTS AND CAPABILITIES

The overriding emphasis of inspection is to provide data on the assembly process that can be used to improve it in a closed-loop manner and not simply to screen the assembly-process output for defects. Therefore, to develop a system to inspect the quality of solder joints using scanned-beam X-ray laminography first requires a proper understanding of the solder-joint features that ensure long-term reliability as well as the possible assembly-process defects that may arise.

A. Technology Description

BGA is an area-array, SMT package-interconnection technique for mounting IC chips on surface-mount PCB's. Referring to Fig. 1, the particular BGA-joint structure investigated in this work consists of 90% Pb/10% Sn solder balls, 0.89 mm in diameter, that are attached to circular pads on the underside of the ceramic chip package at a pitch of 1.27 mm with 63% Sn/37% Pb eutectic solder. The resulting surface-mount package is attached to a PCB by placing it into 63% Sn/37% Pb eutectic solder-paste screened on circular copper pads and reflowing the assembly. During reflow, surface tension minimizes the surface free-energy of the eutectic fillets by dynamically centering the ball between them. The solder ball provides the necessary standoff between the chip package and the PCB to relieve the shear strains induced by the coefficient

of thermal expansion (CTE) mismatch experienced during power cycling.

The most critical feature for maximizing the fatigue life of a BGA joint is the volume of the solder fillet between the ball and the PCB pad (pad fillet), which is characterized by the diameter at its minimum cross-section and must be sufficient to withstand the stresses experienced during power cycling [1]. Furthermore, the centroid of the solder ball should be aligned with the centers of the package and PCB pads to further reduce the joint's susceptibility to fatigue failure. Based on experience with the standard SMT-assembly process and on experience from the recent BGA-assembly process development, the following have been identified as potential BGA-joint defects, Fig. 2.

Low-Solder and Open Conditions: A low-solder BGA joint lacks sufficient solder to properly join the solder ball to the copper pad on the PCB. An open is the extreme form of the low-solder joint in which the solder makes no contact between the ball and the copper pad.

Pad-Nonwet Condition: A pad nonwet is an open or low-solder condition between the solder ball and the PCB pad with the additional increased solder-volume condition between the ball and the pad of the chip package.

Solder Bridges: A solder bridge is any unwanted solder joining a BGA joint to an adjacent joint or via.

Ball/Pad Misalignment: A ball/pad misalignment exists when the horizontal distance between the ball's vertical axis and the pad center is greater than 25% of the pad width.

B. Scanned-Beam X-Ray Laminography (SBXLAM)

The SBXLAM system used in this work was developed specifically to perform the automated inspection of solder joints, Fig. 3 [6], [7]. As the electron beam strikes the tungsten target-anode in SBXLAM, it is electrically scanned or rotated about a fixed axis at 600 RPM synchronously with a rotary detector 180° out of phase, producing a focal plane at a fixed position. Different magnification factors are achieved by changing the scan radius of the X-ray source which, in turn, vertically shifts the focal plane. The system used in this work has two scan radii resulting in magnification factors

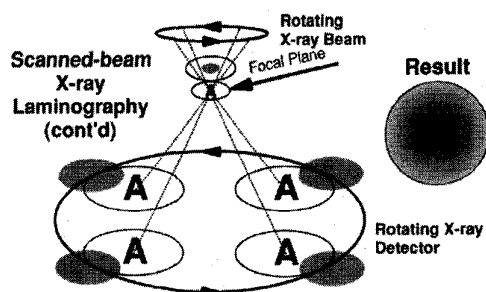


Fig. 3. Focal-plane generation for SBXLAM.

of 9.5 times and 19 times within respective field-of-views (FOV's) of 10.2×9.5 mm and 5.1×4.8 mm, and respective laminographic angles of 28° and 26° . The image formed on the phosphor screen is digitized every 33 ms, resulting in 3 images per revolution. Several of these images or frames must be averaged over one or more complete revolutions of the rotary detector to form the final image for analysis, which results in an inspection rate of 4 to 25 solder joints per second. Each digitized image is 512×480 pixels with 256 gray levels at an image resolution, depending on the size of the FOV, of either $20 \mu\text{m}$ or $10 \mu\text{m}$ per pixel. However, the attainable resolution is limited by the X-ray source focal-spot size, which is fixed at approximately $16 \mu\text{m}$.

The total gray-level intensity of a solder joint within the focal plane is an additive combination of: (a) a background gray-level due to the blurring of features outside the focal plane; and (b) a delta gray-level due to the solder in the focal plane. To determine the delta gray-level for an area of a solder joint due solely to solder in the focal plane, the background gray-level of the region around the joint is subtracted from the average gray-level of the area in the joint.

C. Initial Assessment of SBXLAM

The National Institute of Standards and Technology (NIST) determined empirically that a highly-attenuating sphere can project a distinct image-artifact into a focal plane vertically separated from the sphere's surface by a maximum distance approximately equal to the sphere's radius for a 28° laminographic angle [12], and that the radius of the image-artifact increases as the focal plane moves closer to the sphere. The conjecture that this effect, otherwise known as laminographic "smear," would reduce the SBXLAM system's ability to provide sufficient image contrast and signal-to-noise ratio was confirmed by an examination of the laminographic X-ray images of "open" BGA-joints.

After an initial experimentation phase, it was concluded that the solution lay in minimizing the scattering of low-energy X-ray photons (<50 keV) by the solder balls. Several alternative approaches are available [13], but the only viable approach was to "harden" or increase the mean energy of the X-ray beam, which makes it more penetrating and increases the proportion of directly-transmitted photons to scattered photons [13]. The X-ray beam itself can be hardened by positioning a thin metal filter (a 0.05-mm thick tungsten sheet in our case) normal to its path that preferentially absorbs the low-energy

X-ray photons, improving the overall penetration quality of the X-ray beam.

III. PRELIMINARY EVALUATION OF THE SBXLAM IMAGES OF BGA JOINTS

Two BGA test-vehicles, each with four 32-mm BGA modules having 625 joints each, were assembled for this work. On the first test vehicle, assembled at IBM's Development Lab, then located in Austin, Texas, the exact locations of the defects were mapped to permit proper evaluation and calibration. However, on the second sample, assembled at IBM's Manufacturing Plant in Toronto, Canada, the exact locations of the defects were not recorded. Image-slices were taken at the PCB pad level, 0.13 mm above and below the pad, 0.48 mm above the pad (the approximate location of ball center), and 0.97 mm above the pad (the approximate location of the package fillet).

A. Nominal BGA-Joints

The laminographic X-ray images of nominal BGA-joints were examined to determine characteristic features. The image-slices taken at the pad level, referred to as the pad slice, indicated that the pad fillets were axisymmetric about the base of the solder balls, Figs. 4(a) and 5(a). The 3-D representation of the BGA-joint density within the pad slice revealed a structure resembling a bell that could be discretely characterized by annular rings of constant thickness. The typical diameter of the nominal-joint images, characterized by distinct edges, was approximately 0.71 mm, which is exhibited in the cross-sectional profile shown in Fig. 4(b).

However, an axisymmetric, laminographic smearing of the solder balls was apparent as far as 0.56 mm beyond this distinct edge, contributing substantially to the background gray-level. Furthermore, the vertical position of the solder balls with respect to the pad surface and, hence, the pad slice, affected the overall intensity of the joint images. A pixel gray-level frequency-histogram generated within a circular region centered on the pad and with twice the area of the pad revealed two distinct peaks, Fig. 5(b). The taller peak represents the average background gray-level, and the shorter peak represents the average solder-thickness within the pad, including the effect of the solder ball. It was noted that the additional image-slices 0.13 mm above and below the pad level provided no further information concerning either the Pad fillets or the solder balls than that provided by the Pad Slice.

The joint images in the image-slices taken at 0.97 mm above the pad, referred to as the package slice, had similar intensities as the pad slice for the background gray-levels and delta gray-levels, Fig. 5(c). However, since the package fillets are 15% wider than the pad fillets, a distinct edge defining the boundary between the ball and the package fillet was quite evident.

The image-slice taken at 0.48 mm above the pad, shown in Fig. 5(d), is referred to as the ball slice and is located at the approximate vertical center of the solder balls. No evidence of either the pad fillets or the package fillets existed in this image-slice. Therefore, the ball slice was seen to provide the most reliable information on the horizontal position of the solder

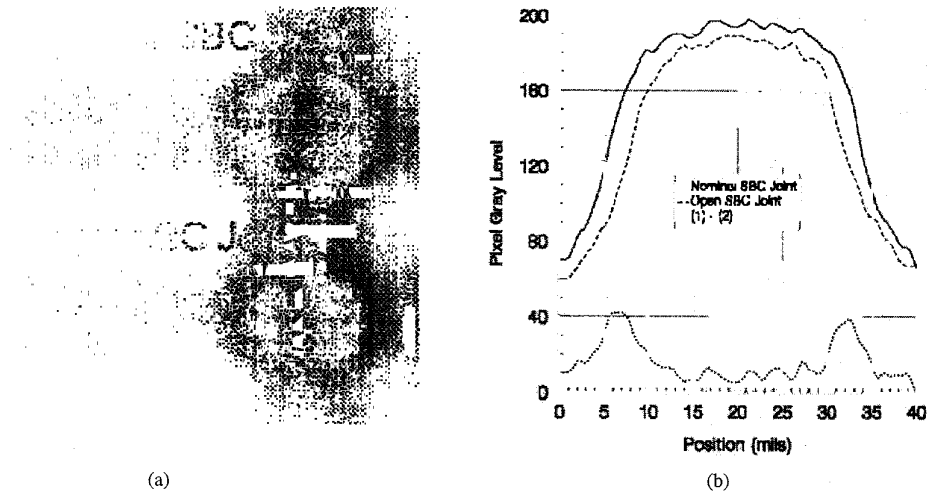


Fig. 4. BGA image-artifacts: (a) X-ray image and (b) centerline gray-scale profiles.

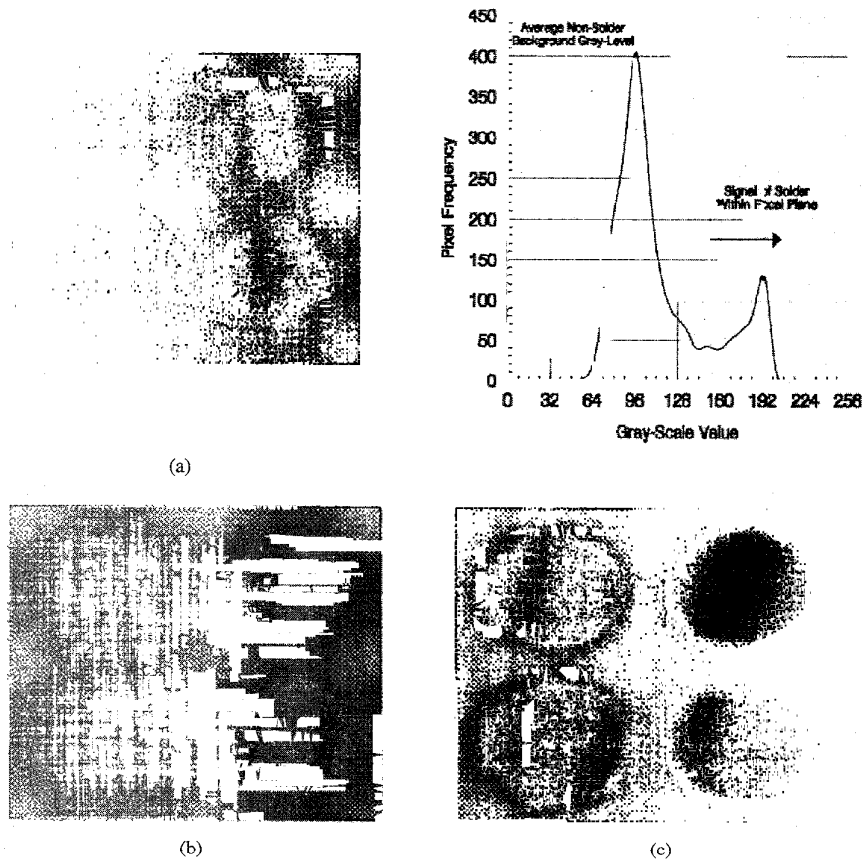


Fig. 5. Nominal and open BGA-joints: X-ray images at the (a) pad slice, (b) ball slice, and (c) package slice.

balls. The ball images in this slice had accurate diameters of 0.89–0.91 mm with very distinct edges and relatively low background gray-levels.

B. Open/Low-Solder Conditions

The pad slice images of open BGA-joints shown in the upper part of Fig. 5(a) were clearly distinguished from the nominal BGA-joints as having much smaller diameters. The

(dark) circular area still seen in the pad slice image for an open joint is due entirely to the presence of the solder ball. The average diameter of this “virtual image” was approximately 78% of that for a nominal BGA-joint, Fig. 4(b). Thus, the most significant difference between an open joint and a nominal joint in the joint’s delta gray-level can be observed at the pad perimeter. The average delta gray-level measured in an annular ring at the pad perimeter was as much as 30% less than a similar measurement of a nominal BGA-joint.

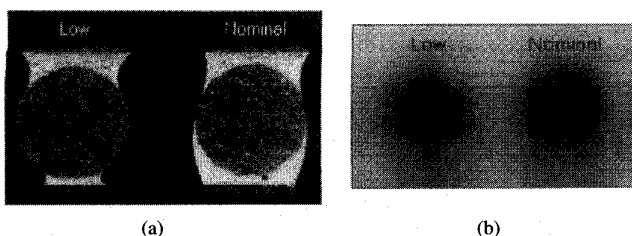


Fig. 6. Low-solder BGA-joint: (a) physical cross-section and (b) X-ray image at pad slice.

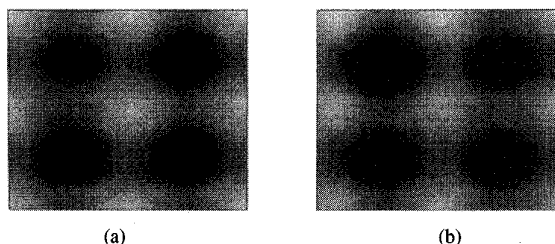


Fig. 7. Pad nonwet: X-ray images at (a) pad slice, and (b) package slice.

Low-solder BGA joints were not as clearly distinguished from the nominal BGA-joints in the X-ray images at the pad slice, as were the open joints, Fig. 6. The apparent joint diameters ranged from 85–94% of the nominal solder-joint diameters, and the delta gray-levels at the pad perimeter were up to 25% lower than for a nominal BGA-joint. Furthermore, the actual feature which defines a low-solder condition, namely the minimum fillet-diameter, could not be directly measured due to the laminographic smearing of the solder ball. The low-solder condition, therefore, can only be inferred by measuring the average joint-diameter, defined by the outer edge of the joint image, and the average solder thickness at the pad perimeter, represented by the delta gray-level and the background gray-level. As with the nominal BGA-joints, the additional image-slices 0.13 mm above and below the pad level provided no further information.

C. Pad Nonwets

The image of a pad nonwet, the upper left joint in Fig. 7(a), has the same features as an open/low-solder BGA-joint at the pad slice, and a larger joint-diameter and a higher delta gray-level than a nominal joint, at the package slice, Fig. 7(b). Therefore, measurements taken at the package slice of the package fillet can be used to distinguish an open/low-solder condition from a pad nonwet.

D. Ball/Pad Misalignment

Ball/pad misalignments were clearly evident in the pad slice, shown in Fig. 8(a), with the two joint images in the lower left having elliptic rather than circular shapes. Since the ball slice provides the best opportunity for accurately determining the horizontal position of the solder ball, Fig. 8(b), the ball slice must be processed to determine the ball center. As well, the presence of a solder bridge and its effect on the offset

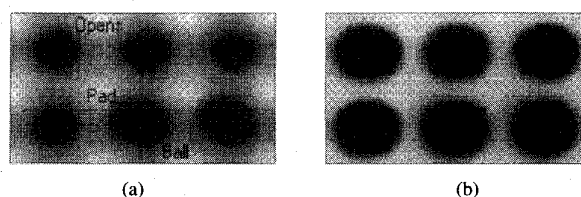


Fig. 8. Ball/pad misalignment: X-ray images at (a) pad slice, and (b) ball slice.

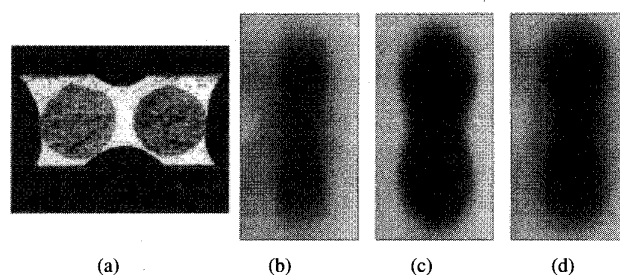


Fig. 9. Major solder-bridge: (a) physical cross-section, and X-ray images at the levels of the (b) pad slice, (c) ball slice, and (d) package slice.

measurement must be considered when the algorithm is being developed.

E. Solder Bridges

Major bridges on all image-slices, shown in Fig. 9, had delta gray-levels equal to those of the joint images and were at least as wide as the joint images. Consequently, the major bridges can easily be found by measuring the delta gray-level above the average background gray-level in small regions outside the joint area along the principal directions toward adjacent BGA-joints. The features of the minor bridges are also visible on all image-slices as shown in Fig. 10, with distinct edges and a delta gray-level sufficiently higher than the surrounding background to locate them.

IV. DEVELOPMENT OF THE INSPECTION ALGORITHMS

A. Measurement of Key BGA Features

From the examination of the laminographic X-ray images of nominal and defective BGA-joints in Section 3.0, the key features that characterize BGA joints, and the image-slices in which to measure them, are defined as:

- (a) Ball/Pad offset (ball and pad slices); and,
- (b) Average solder-thickness at perimeter and average joint-diameter (pad and package slices).

Furthermore, measurements must be taken in the region surrounding the BGA joints to check for bridges.

In order to maintain efficiency, thus speed, the inspection algorithms were developed utilizing a library of available low-level image-processing primitives in the SBXLAM system to locate features and perform the actual measurements in the gray-scale images of the solder joints. The primitives operate within either a rectangular or circular region-of-interest (ROI) defined by the algorithms according to the CAD data for the particular PCB assembly.

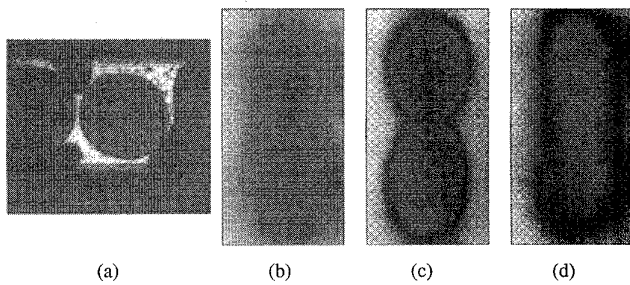


Fig. 10. Minor solder-bridge: (a) physical cross-section, and X-ray images at the levels of the (b) pad slice, (c) ball slice, and (d) package slice.

Many of the critical BGA-joint features are required in the identification of more than one defect. Thus, the first algorithm, referred to as MEASURE, to analyze the current FOV takes all the measurements necessary to characterize the BGA joints and makes them available to the subsequent defect-identification algorithms.

1) *Location of Solder-Ball Centroid in the XY-Plane (Ball Slice)*: Since the solder ball can move in any direction to minimize the surface free-energy of the pad and package fillets, its centroid must be located to properly adjust the positions of the ROI's for all subsequent measurements. Three basic image-processing primitives are used sequentially in the following procedure to locate the ball centroid within the ball slice:

- (i) A circular ROI is centered at the pad centroid defined by the CAD data. Its radius is equal to the pad radius plus half the distance between adjacent pads.
- (ii) From the centroid position, eight spokes are extended to the edge of a circular ROI with a diameter at least 20% greater than the nominal ball-diameter. The slope is calculated along each spoke, and the ball edge is located based on an edge threshold. The eight edge-points are then used for the second estimate of the ball centroid and its radius by applying the technique developed by Thomas and Chan [14].
- (iii) A rectangular donut operator is then used to locate the position of the maximum average solder-thickness as the final estimate of the ball centroid. As the donut operator is centered sequentially on each pixel along a defined straight path, the difference between the average gray-levels in the outer region and the inner region of the operator is calculated for each of these pixels. The pixel which has the maximum negative difference is the position of the maximum average solder-thickness. To make the final estimate of the ball centroid, the donut operator is first run in the X direction, centered at the second estimate of the ball centroid, and then, in the Y direction, centered at the adjusted X from the first pass and the Y of the second estimate of the ball centroid. The pixel identified in the final pass of the donut operator is then used as the position of the ball centroid.

MEASURE subsequently calculates the distance between the "projected" ball centroid and the CAD-specified pad centroid, that is, the ball/pad offset.

2) *Measurement of Local Background Gray-Level (Pad and Package Slices)*: The measurement algorithm determines a

local background gray-level for each eutectic fillet. From a frequency histogram generated inside a circular ROI that circumscribes both the pad and the ball, Fig. 5(a), the weighted average gray-level is calculated for the "background" [pixels with the lowest gray-levels, represented by the taller peak in Fig. 5(b)]. This value is stored as the local background gray-level in the global data-area. The second, shorter peak in Fig. 5(b) represents the solder in the pad region. The weighted average of this peak is used to calculate the average solder-thickness for the pad region.

3) *Measurement of Ring-Structure Characteristics (Pad and Package Slices)*: The solder distribution in a BGA joint shown in Fig. 11 is characterized by three ring regions. The solder thickness in the central ball region is a good indicator of the proximity of the ball to the focal plane and can be used to normalize the other solder-thickness measurements to account for this. However, the variation in solder thickness between low and nominal solder-joints is most evident in the outer ring-region.

Fig. 11 represents the ideal case if the ball is aligned with the pad. However, if the ball is offset from the pad, the solder fillet will skew toward the ball, though the annular ring-structure will still be evident. Therefore, the average solder-thickness is measured in three circumjacent rings centered with respect to the offset between the ball centroid and the pad centroid. These measurements are taken using the following procedure:

- (i) The average solder-thickness is measured in the ball region of the BGA joint within a circular ROI having a radius approximately 55% of the pad radius.
- (ii) The average solder-thickness is then measured between the ball region and the pad perimeter within an inner-ring ROI and an outer-ring ROI. Unless the ball and pad centroids coincide, the centers of the circles which define the limits of each annular measurement region do not coincide. Instead as their radii increase, the circles are centered progressively toward the pad centroid along the line segment between the ball and pad centroids to account for the fillet being skewed by any offset of the solder ball from the pad centroid. The radii of inner ring and the outer ring are approximately 85 and 115% of the pad radius respectively.

4) *Determination of Solder-Fillet Extent (Pad and Package Slices)*: To characterize the extent of the solder on the pad, the following solder-fillet measurements are taken:

- (i) The first measurement shown in Fig. 12 traces a contour around the perimeter of the solder joint connecting all pixels with the same gray-level within a defined circular ROI. The contour level specifies the total gray-level, (i.e., the additive total of both the background and delta gray-levels), that corresponds to the approximate solder-thickness at the edge of the minimum cross-section of the fillet. The physical cross-sections of nominal and defective BGA-joints revealed that the solder thickness at the edge of the minimum fillet cross-section is typically between 0.05–0.08 mm or about 50–60% of the average solder thickness. The pixels that lie on the contour are then used to estimate the diameter and center of the solder fillet [26].

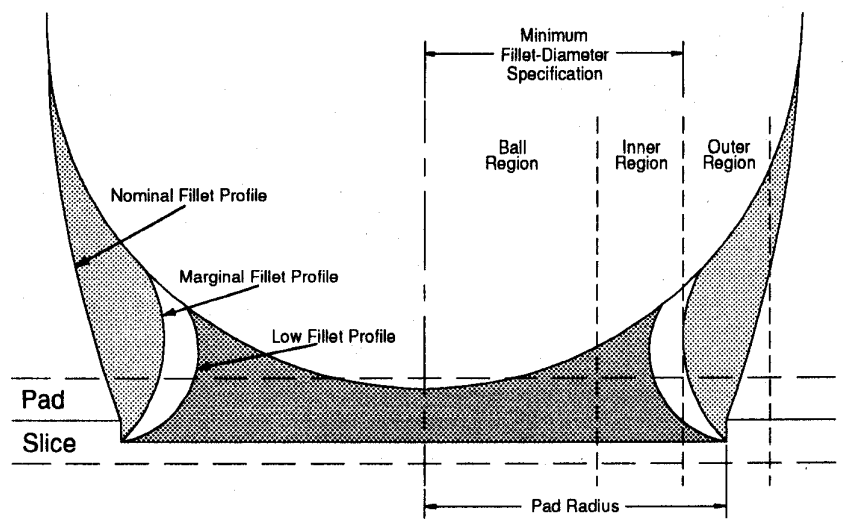


Fig. 11. Cross-section of BGA ring-structure for aligned solder ball.

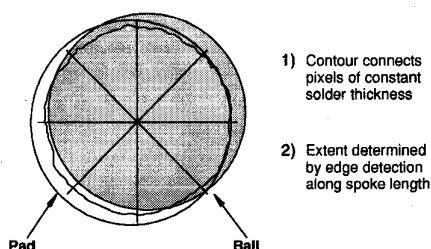


Fig. 12. Solder-fillet contour and extent.

- (ii) Contour tracing requires a constant background gray-level around the entire BGA joint, which is not always the case. Therefore, an additional measurement is taken using spoke edge-detection to locate the edge of the solder fillet. From the midpoint of the line segment between the pad centroid and the ball centroid, eight spokes are extended to the edge of a circular ROI that circumscribes the ball and the pad, Fig. 12. The solder-fillet edge is located along each of the eight spokes. As with the contour pixels, the eight edge-pixels are used to determine the average diameter or extent of the solder fillet [14]. Unlike (i), this measurement is not dependent on the solder-thickness calibration.

B. Open/Low-Solder Identification Algorithm

The algorithm for identifying an open or low-solder condition uses the following (in comparing to their thresholds) to determine whether an open/low-solder condition exists at a BGA joint:

- (i) Average solder-thickness on the pad, Section IV-A-2.
- (ii) Average solder thickness in the ball region, and in the inner and outer rings around the ball region, Section IV-A-3.
- (iii) Average diameters of the solder-fillet contour, Sections IV-A-4.
- (iv) Ratio of the outer-ring thickness multiplied by the inner-ring thickness and divided by the ball-region thickness, herein referred to as the outer-inner-ball (OIB) ratio.

C. Pad-Nonwet Identification Algorithm

If an open/low-solder condition exists at the pad slice for a BGA joint, the pad-nonwet algorithm then uses the same measurements and the OIB ratio as the open/low-solder algorithm, though taken at the package slice, to identify an excess-solder condition. If any one of the measurements or the OIB ratio is greater than its threshold, the algorithm classifies the joint as having a pad-nonwet condition.

D. Ball/Pad Misalignment Identification Algorithm

The algorithm for identifying a ball/pad misalignment compares the distance between the ball centroid and the pad centroid to the user-defined maximum ball/pad offset to determine whether the ball is misaligned. The maximum user-defined threshold is specified as a percentage of the pad width.

E. Solder-Bridge Identification Algorithm

1) *Check for Major Bridges:* The algorithm checks for major bridges in the following manner:

- (i) Eight square ROI's are defined around the joint along an ellipse that circumscribes both the ball and the pad, Fig. 13. The solder thickness is measured in each ROI and compared to a defined threshold.
- (ii) If the solder thickness is greater than the threshold, the spoke edge-detection technique, described in Section IV-A-1, is used to find the longitudinal edges of the bridge and determine the width of the bridge.
- (iii) The spoke edge-detection is also used to find the length of the bridge to ensure that the bridge extends to an adjacent BGA-joint or to an interstitial via. The bridge width and extent are then compared to user-defined thresholds, and if both measurements are greater than the thresholds, a major bridge is identified. If no major bridges are found, the algorithm continues with the next check for minor bridges.

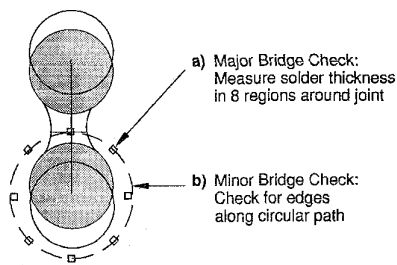


Fig. 13. Solder-bridge checks.

2) *Check for a Minor Bridge:* The algorithm checks for minor bridges in the following manner:

- (i) A circular ROI shown in Fig. 13 is defined outside the ball/pad area, with its center at the midpoint of the line segment between the ball centroid and the pad centroid and its circumference passing through the midpoint of the line segment between the pad centroid and the centroid of the adjacent pad nearest the ball. The slope is then calculated along the path to locate local slope-extrema with absolute values greater than a defined threshold, indicating possible edges of solder bridges. When locating local slope-extrema, consecutive slope maxima and minima are paired together as the endpoints of a line segment under the assumption that they indicate leading and trailing edges of solder bridges. Only those local slope-extrema pairs that meet a minimum height/width ratio are selected.
- (ii) For each local slope-extrema pair returned by the edge search, the width of the bridge and its angular displacement relative to the pad centroid are determined. As with the major-bridge check, the spoke edge-detection technique is used to find the extent of the bridge to ensure that the bridge extends to an adjacent BGA-joints or to an interstitial via. The bridge width and extent are compared to user-defined thresholds, and if both measurements are greater than the thresholds, a minor bridge is identified; otherwise, if the bridge width is greater than the threshold but the bridge does not extend completely between joints, a further check is performed.
- (iii) The contour-tracing technique described in Section IV-A-4 is used to measure the extent of the solder within a square ROI that extends to the centroids of all 8 adjacent BGA-joints. The contour gray-level is set to the average gray-level between the two edges. If the solder contour reaches the perimeter of an adjacent joint or an interstitial via, a minor bridge is identified.

V. EVALUATION OF THE INSPECTION ALGORITHMS FOR BGA

To evaluate the performance of automated-inspection systems, the electronics-manufacturing industry has established four performance-criteria [15]: the false-alarm rate, the escape rate, the inconsistency rate, and the inspection rate. The established industry-standard levels for these performance criteria for the automated inspection of high-reliability products are better than 0.2% for the false-alarm rate, 2% for the escape rate, and 3% for the inconsistency rate [15].

A. Establishment of the Number of Frame Averages and the FOV Size

Increasing the number of frame averages and reducing the FOV size both decrease the signal-to-noise ratio of the laminographic image. However, the inspection time increases with the number of frame averages and a reduced FOV. Therefore, a balance must be established between the inspection time and the signal-to-noise ratio. From experimentation, the optimum balance for imaging the BGA joints was achieved using 12 frame averages in the 5.1×4.8 mm FOV, providing an inspection rate of 5 joints per second.

B. Performance Evaluation—Initial Results

To both establish the accept/reject thresholds and initially evaluate the effectiveness of the algorithms developed to inspect and measure the characteristics of BGA joints, four samples, each with 625 joints, were inspected on the SBXLAM system.

1) *Solder-Thickness Calibration:* The solder-thickness calibration plate consisted of: nine solder discs, 1.27 mm in diameter, ranging in thickness from 0.04 mm to 0.61 mm; and, four groups of four discs, 1.27 mm in diameter and 0.18 mm thick, each covered by different thicknesses of copper, 0, 0.13, 0.25, and 0.38 mm, respectively, to simulate different background gray-levels. Using the camera settings established for the BGA assemblies and with the 0.05-mm tungsten filter over the calibration plate, an additional 0.075–0.10 mm lead sheet was added over the plate to achieve the same background and delta gray-level ranges as the BGA assemblies. The first part of the solder-thickness calibration procedure consisted of measuring the delta gray-levels for the nine different solder-thicknesses with a constant background gray-level. The second part consisted of measuring the delta gray-level for a constant solder-thickness at four different background gray-levels spread evenly across the background gray-level range. The second calibration provides a scaling factor to adjust the first calibration curve based on the background gray-level.

2) *Solder-Joint Feature Measurements:* Once the solder-thickness calibration had been performed, all of the BGA joints on the samples were fully characterized by the initial measurement-algorithm to determine the values of the solder-joint features used to identify the open/low-solder conditions and the pad nonwets. Table I summarizes the data from the initial characterization process.

3) *Comparison to Physical Cross-Section Measurements:* After the BGA samples were fully characterized, they were physically cross-sectioned and photographed with a high-magnification lens. The diameters of the minimum fillet cross-sections were measured from the photographs and compared to the solder-joint feature-measurements from the X-ray images. The physical cross-sections of the open/low-solder samples confirmed that there were 52 nonwet or open BGA joints. Moreover, there were 83 low-solder BGA joints. However, as illustrated in Table II, the low-solder joints were not as dissimilar in their feature-measurements in the X-ray images from the population of good joints as were the open joints.

TABLE I
FEATURE-MEASUREMENTS OF THE PAD SOLDER-FILLET

Feature	μ_F	σ_F	σ_M	Lowest Good Joint	Range of Low-Solder Joints (85 joints)	Range of Opens (50 joints)
Outer Ring	0.094	0.012	0.003	0.061(2.8 σ)	0.049(3.8 σ) - 0.071(2.0 σ)	0.036(5.0 σ) - 0.050(3.7 σ)
Inner Ring	0.274	0.037	0.010	0.179(2.6 σ)	0.118(4.2 σ) - 0.206(1.8 σ)	0.088(5.0 σ) - 0.129(3.9 σ)
Ball Region	0.606	0.057	0.013	0.343(4.6 σ)	0.316(5.1 σ) - 0.504(1.8 σ)	0.237(6.5 σ) - 0.337(4.7 σ)
Avg Thickness	0.324	0.055	0.013	0.207(2.1 σ)	0.175(2.7 σ) - 0.237(1.6 σ)	0.135(3.5 σ) - 0.179(2.6 σ)
Avg Radius	0.345	0.008	0.002	0.316(3.4 σ)	0.292(6.3 σ) - 0.329(1.8 σ)	0.262(9.9 σ) - 0.293(6.2 σ)

TABLE II
PAD SOLDER-FILLET FEATURE-MEASUREMENTS CONFIRMED BY CROSS-SECTIONING (VALUES ARE IN mm)

Feature	Lowest Good Joint (1)	Range (2) of Low-Solder Joints (83 joints)	# Good Joints in Range (2)	# Low-Solder Joints > (1)	Accept/Reject Threshold	Threshold for Open Joints
Outer Ring	0.061(2.8 σ)	0.049(3.8 σ) - 0.076(1.6 σ)	45	52	0.073(1.8 σ)	0.051(3.7 σ)
Inner Ring	0.179(2.6 σ)	0.118(4.2 σ) - 0.233(1.1 σ)	69	53	0.222(1.4 σ)	0.130(3.9 σ)
Ball Region	0.343(4.6 σ)	0.316(5.1 σ) - 0.587(0.4 σ)	98	63	0.502(1.7 σ)	0.337(4.7 σ)
Avg Thickness	0.207(2.1 σ)	0.175(2.7 σ) - 0.260(1.2 σ)	57	52	0.247(1.4 σ)	0.179(2.6 σ)
Avg Radius	0.316(3.4 σ)	0.292(6.3 σ) - 0.331(1.6 σ)	44	53	0.330(1.8 σ)	0.293(6.1 σ)

TABLE III
SUMMARY OF PERFORMANCE RESULTS FOR DEFECT IDENTIFICATION-ALGORITHMS

Defect Type	Sample Size Total Joints (Defects)	False-Alarm Rate	Escape Rate	Inconsistency Rate
Initial Results:				
Solder Bridges	1250 (50)	0.17% (2/1200)	0.0% (0/50)	0.048% (6/12500)
Ball/Pad Misalignment	1250 (39)	0.25% (3/1211)	0.0% (0/39)	0.17% (21/12500)
Open (O) / Low-Solder (LS)	1250 (52 O and 83 LS)	3.1% (35/1115)	6.7% (9/135)	0.82% (103/12500)
Open Joints	1250 (52)	0.42% (5/1198)	0.0% (0/52)	0.15% (19/12500)
Improved Results with Multiple Camera-Settings and OIB Ratio:				
Open/Low-Solder	3750 (40 O and 150 LS)	1.4% (50/3560)	2.6% (5/190)	0.48% (179/37500)
Open Joints	3750 (40)	0.11% (4/3710)	0.0% (0/40)	0.040% (15/37500)
Pad Nonwets	2500 (50)	0.82% (20/2450)	2.0% (1/50)	0.29% (72/25000)
Final Results with Revised Solder-Thickness Calibration:				
Open/Low-Solder	3750 (40 O and 150 LS)	0.87% (31/3560)	2.1% (4/190)	0.38% (142/37500)
Open Joints	3750 (40)	0.081% (3/3710)	0.0% (0/40)	0.029% (11/37500)
Pad Nonwets	2500 (50)	0.37% (9/2450)	0.0% (0/50)	0.18% (45/25000)

The accept/reject thresholds for the open/low-solder identification-algorithm shown in the sixth column of Table II were established to minimize both the escape rate and the false-alarm rate. Referring to Table III, the open/low-solder algorithm did not perform very well using these thresholds, having (false-alarm, escape, and inconsistency rates) of (3.1%, 6.7%, and 0.82%). However, if the accept/reject thresholds were set to identify only open joints, as shown in the seventh column of Table II, the algorithm performed very well, correctly identifying all opens, with a false alarm rate of only 0.42%.

4) *Discussion of Initial Results of Open/Low-Solder Algorithm:* All 44 BGA joints that were incorrectly classified had

minimum fillet-diameters within ± 0.025 mm of the minimum specification limit. Therefore, the poor performance of the open/low-solder identification algorithm was likely due to a low signal-to-noise ratio reducing the ability to make fine distinctions in the fillet diameters of BGA joints close to the minimum specification limit. This can be attributed to three factors: the shadowing of the eutectic fillet by the solder ball, the variable proximity of the solder ball to the image plane, the camera settings, and the solder-thickness calibration technique. Other than using the tungsten filter to harden the X-ray beam, nothing further can be done feasibly to reduce the shadowing of the solder ball, and, therefore, attention was directed toward the other two factors.

C. Performance Evaluation with Multiple Camera Settings

Because of the large variation in gray-level intensity using the same camera settings across the entire module it was decided that the two outermost rows of BGA joints should have different camera settings and the corresponding different solder-thickness calibration than the ones for the interior BGA joints. Therefore, the combined effectiveness of using multiple camera-settings and the OIB normalization ratio was tested using a new sample consisting of 6 BGA modules. The pad-nonwet identification-algorithm was tested for the first time during this evaluation since the previous sample was not properly prepared to generate true pad-nonwets. It performed within specification as shown in Table III, though the escape rate was 2.0%.

Using multiple camera-settings and the OIB ratio, but only one set of accept/reject thresholds, the performance of the open/low-solder identification-algorithm did improve by more than 50% but still was not within specification as shown in Table III. However, with separate accept/reject thresholds set to identify only open joints, the false alarm and inconsistency rates of the identification algorithm improved by almost 75%.

D. Performance Evaluation with a Revised Solder-Thickness Calibration Technique

The original calibration technique relied on a lead sheet, 0.075–0.10 mm thick, covering the calibration plate to simulate the effect of the solder balls on the solder-thickness measurements of the eutectic fillets above and below the balls. A more accurate approach would be to attach an actual solder ball to each solder disc of known thickness.

Accordingly, 280 solder discs (8 groups of 35 discs) with respective thicknesses of 0.03, 0.05, 0.08, 0.10, 0.15, 0.20, 0.25, and 0.30 mm were attached to the copper pads of 8 BGA sites, each site having 35 discs of the same thickness. At each site, 17 discs were attached to pads along the perimeter, and 18 discs were attached to pads throughout the interior. A BGA module was then attached with a thin layer of adhesive to each site.

The effectiveness of the revised solder-thickness calibration technique was evaluated using the same sample of 6 BGA modules. The revised calibration technique reduced the variability of the solder-joint feature-measurements, thereby improving the performance of the open/low-solder identification-algorithm by more than 20% as shown in Table III, though the false-alarm and escape rates still did not meet the specifications for production inspection systems. Nevertheless, the performance of the pad-nonwet identification-algorithm and the open algorithm were also improved. However, the improvement in the performance of the open/low-solder identification-algorithm is still insufficient to consider using the X-ray laminography system to inspect BGA joints for marginally low-solder joints.

VI. CONCLUSION

Developing an inspection process for the BGA technology presents a significant challenge since the majority of reflowed

solder-fillets are occluded by the solder balls and the ceramic substrate. Scanned-beam X-ray laminography (SBXLAM) was determined to be the only available, automated solder-inspection system realistically capable of evaluating the quality of BGA joints. However, despite the SBXLAM system's ability to focus on a horizontal plane, out-of-plane axisymmetric features with sufficient density, such as the high-lead-content solder balls, can produce large image-artifacts within the focal plane. The use of a 0.05-mm tungsten sheet to filter the low-energy X-ray photons and increase its mean energy was found to significantly reduce the effect of the solder-ball image-artifacts on the fillet images and, thereby, improve the contrast within the fillet images.

The ability of the inspection algorithms to perform the tasks of measurement and classification of BGA joints was evaluated by inspecting BGA modules with defects that were independently verified. The algorithms did perform very well in identifying ball/pad misalignments, bridges, pad-nonwets, open joints, and "very" low-solder joints, and are currently being used in production for such purposes.

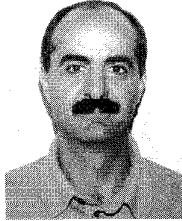
REFERENCES

- [1] G. Phelan and S. Wang, "Solder ball connection reliability model and critical parameter optimization," in *IEEE Proc. 43rd Electronic Comp. and Technol. Conf.*, June 1993, pp. 858–862.
- [2] M. R. Driels and D. J. Nolan, "Automatic defect classification of printed wiring board solder joints," *IEEE Trans. Comp., Hybrids, Manufact. Technol.*, vol. 13, no. 2, pp. 331–340, June 1990.
- [3] Y. G. Lu, L. Z. Jiang, L. X. Zou, W. Z. Geng, and J. Hong, "The inspection of solder joints on printed circuit boards by phase shift holographic interferometry," *NDT Int.*, vol. 23, no. 3, pp. 157–160, June 1990.
- [4] L. J. Santangelo and L. W. Kessler, "Acoustic microscopy: A key inspection tool for improving the reliability of surface mount capacitors and plastic IC packages," *Surface Mount Technology*, Sept. 1989.
- [5] G. Goss, "Developments in advanced X-ray imaging for the automated inspection of electronic assemblies," in *Proc. Test Engineering Conf. 1991*, June 1991, pp. 193–205.
- [6] C. McBee, "Scanned-beam laminography," *Circuits Manufacturing*, pp. 67–69, Jan. 1989.
- [7] B. D. Baker, R. L. Corey, J. A. Adams, and E. W. Ross, "Automated laminography system for inspection of electronics," U.S. Patents 4926452 (May 15, 1990), 5081656 (Jan. 14, 1992), and 5097492, (Mar. 17, 1992).
- [8] M. Koide, "Inspecting connections of multiple component layers on ceramic boards," in *Proc. Technical Program, NEPCON East '91*, June 1991, pp. 75–83.
- [9] T. Sack, "The qualification and implementation of an X-ray laminography inspection system," in *Proc. Technical Program, NEPCON East '91*, June 1991, pp. 40–50.
- [10] A. Jones, M. Lamar, and M. Strnad, "X-ray inspection of SIMM's," *Circuits Assembly*, pp. 44–46, Aug. 1991.
- [11] A. Mitu, S. Rooks, B. Benhabib, and K. C. Smith, "A prototype inspection process for high-density solder-interconnection technologies," in *ASME Proc. Winter Annual Meeting*, Dec. 1991, vol. 50, pp. 141–146.
- [12] T. A. Siewert, M. W. Austin, G. K. Lucey, and M. J. Plott, "System evaluation and qualification standards for an X-ray laminography system," in *Proc. Technical Program, NEPCON East '91*, June 1991, pp. 51–64.
- [13] T. S. Curry III, J. E. Dowdey, and R. C. Murry Jr., *Christensen's Introduction to the Physics of Diagnostic Radiology*, 4th ed. Philadelphia: Lea and Febiger, 1990.
- [14] S. M. Thomas and Y. T. Chan, "A simple approach for the estimation of circular arc center and its radius," *Computer Vision, Graphics, and Image Processing*, no. 45, pp. 362–370, 1989.
- [15] *User's Guidelines for Automated Solder Joint Inspection Systems*, IPC-AI-641, The Inst. Interconnecting and Packaging Electronic Circuits, Jan. 1987.



S. M. Rooks received the B.A.Sc. and M.A.Sc. degrees in mechanical engineering from the University of Toronto.

After his graduation in 1990, he worked at Celestica on solder-joint-inspection issues until 1994. He is currently completing his M.B.A. degree at Stanford University and consulting part-time. He has published numerous articles and has one pending patent application.



B. Benhabib (M'93) received the Ph.D. degree in mechanical engineering from the University of Toronto, Canada, in 1985.

He is currently an Associate Professor in the Department of Mechanical Engineering at the University of Toronto. His research interests are in the general area of computer-integrated manufacturing.

Dr. Benhabib is a senior member of the SME, as well as member of ASME, and AAAI. He is a registered Professional Engineer.



K. C. Smith (S'53-A'54-M'60-SM'76-F'78) received the Ph.D. degree in physics from the University of Toronto, Canada, in 1960.

He is currently a Professor in the Department of Electrical and Computer Engineering at the University of Toronto. He is also cross-appointed to the Departments of Mechanical Engineering, Computer Science, and Information Studies. His research interests include analog VLSI, multiple-valued logic, and flexible manufacturing.

Dr. Smith was elected Fellow of the IEEE in 1978 for "Contributions to Digital Circuit Design." He is presently (1993-1995) a Visiting Professor at the Department of Electrical and Electronic Engineering, Hong Kong University of Science and Technology.